

Quantum Melting of Spin Ice: Emergent Cooperative Quadrupole and Chirality

Shigeki Onoda and Yoichi Tanaka

Condensed Matter Theory Laboratory, RIKEN, 2-1, Hirosawa, Wako 351-0198, Saitama, JAPAN

(Dated: February 3, 2022)

A quantum melting of the spin ice is proposed for pyrochlore-lattice magnets $\text{Pr}_2\text{TM}_2\text{O}_7$ ($\text{TM} = \text{Ir}$, Zr , and Sn). The quantum superexchange Hamiltonian having a nontrivial magnetic anisotropy is derived in the basis of atomic non-Kramers magnetic doublets. The ground states exhibit a cooperative ferroquadrupole and pseudospin chirality, forming a magnetic analog of smectic liquid crystals. Our theory accounts for dynamic spin-ice behaviors experimentally observed in $\text{Pr}_2\text{TM}_2\text{O}_7$.

PACS numbers: Valid PACS appear here

It has been a great challenge to realize unconventional spin-liquid states in three-dimensional magnets. It is achieved by preventing a dipole long-range order (LRO) of magnetic moments, which requires appreciable quantum spin fluctuations and geometrical frustration of magnetic interaction [1–4]. The importance of the geometrical frustration is manifest as in pyrochlore systems [5–8]. In particular, in the dipolar spin ice $R_2\text{Ti}_2\text{O}_7$ ($R = \text{Dy}$ or Ho) [6–8], the rare-earth magnetic moment located at each vertex of tetrahedrons points either inwards (“in”) to or outwards (“out”) from the center (Fig. 1 (a)). The nearest-neighbor ferromagnetic coupling mainly due to the magnetic dipolar interaction favors macroscopically degenerate “2-in, 2-out” configurations without any LRO, forming a magnetic analog of the water ice [8]. Then, the classical spins are quenched into one of the degenerate ground states [9]. Usually, a thermal heating is required for melting the quenched spin ice. Here, we pursue an alternative possibility that quantum fluctuations melt the spin ice: the quantum entanglement among degenerate states lift the macroscopic degeneracy, suppress the spin-ice freezing, and lead to a distinct ground state.

A realistic approach to the quantum melting of the spin ice is to choose a rare-earth ion with fewer f electrons and a smaller magnetic moment, e.g., Pr^{3+} . In rare-earth ions with fewer f electrons, the $4f$ wavefunction is spatially extended [10] and can then be largely overlapped with the O $2p$ orbitals at the O1 site (Fig. 1 (a)) in the pyrochlore lattice. Besides, for Pr^{3+} ions, the magnetic dipolar interaction, which is proportional to the square of the moment size, is reduced by an order of magnitude to 0.1 K between the nearest-neighbor sites, in comparison to that for Dy^{3+} ions. Then, the superexchange interaction due to virtual f - p electron transfers, which provides a source of the quantum nature, is expected to play crucial roles in $\text{Pr}_2\text{TM}_2\text{O}_7$ (TM : a transition metal).

Recent experiments on $\text{Pr}_2\text{Sn}_2\text{O}_7$ [11], $\text{Pr}_2\text{Zr}_2\text{O}_7$ [12], and $\text{Pr}_2\text{Ir}_2\text{O}_7$ [13] have shown that the Pr^{3+} ion provides the $\langle 111 \rangle$ Ising moment described by a non-Kramers magnetic doublet. As in the spin ice, any magnetic dipole LRO is absent [11–16]. $\text{Pr}_2\text{Ir}_2\text{O}_7$ shows a metamagnetic transition only when the magnetic field is applied in the $\langle 111 \rangle$ direction [14], indicating the ice-rule formation due

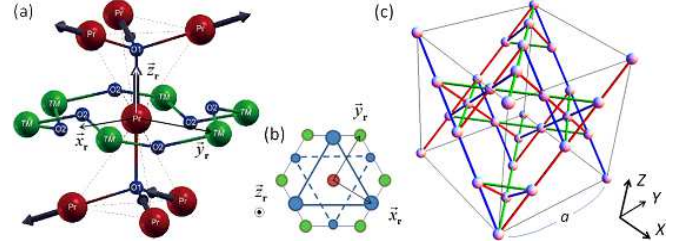


FIG. 1: (Color) (a) Pr^{3+} ions (red) form tetrahedrons (dashed lines) centered at O^{2-} ions (O1) (blue), and are surrounded by O^{2-} ions (O2) (blue) in the D_{3d} symmetry as well as by TM ions (green). Each Pr magnetic moment (bold arrow) points to either of the two neighboring O1 sites. (b) The local coordinate frame ($\vec{x}_r, \vec{y}_r, \vec{z}_r$) from the top. Upward and downward triangles of the O^{2-} ions (O2) are located above and below the hexagon of the TM ions. (c) The Pr pyrochlore lattice. The phase $\varphi_{r,r'}$ in Eq. (2) depends on the color of the bonds. The global coordinate frame (X, Y, Z) is also shown.

to a ferromagnetic coupling $J \sim 1.4$ K [14]. On the other hand, the Curie-Weiss temperature T_{CW} is antiferromagnetic for the zirconate [12] and iridate [13], unlike the spin ice. The stannate shows a significant level of low-energy short-range spin dynamics [15], which is absent in the classical spin ice. Furthermore, the iridate shows the Hall effect at zero magnetic field without magnetic dipole order [14], suggesting an onset of a chiral spin liquid [3] at a temperature $\sim J$ due to quantum fluctuations.

In this Letter, we derive the realistic effective model for Pr $4f$ moments on the pyrochlore lattice. It contains appreciable quantum nature leading to a cooperative ferroquadrupolar ground state, accompanied by crystal symmetry lowering from cubic to tetragonal and a frustration in the chirality ordering. Our scenario explains unusual magnetic properties observed in $\text{Pr}_2\text{TM}_2\text{O}_7$ suggesting a dynamically fluctuating spin ice [14–16].

We start with f^2 configurations for Pr^{3+} forming the tetrahedron centered at the O^{2-} ion (O1) in $\text{Pr}_2\text{TM}_2\text{O}_7$ (Fig. 1). The LS coupling gives the ground-state manifold 3H_4 . Each Pr^{3+} ion is placed in a crystalline electric field (CEF) which has the D_{3d} symmetry about the $\langle 111 \rangle$ direction toward the O1 site. It is useful to define the lo-

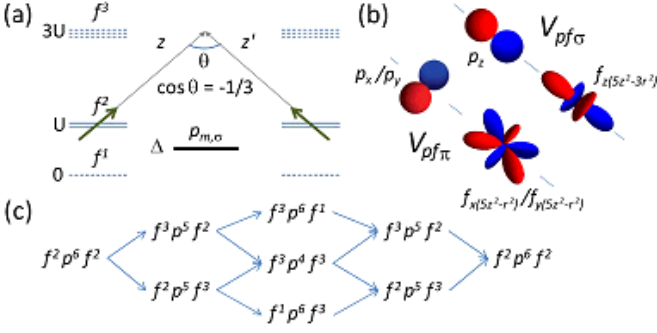


FIG. 2: (Color online) (a) Local level scheme for f and p electrons, and the local quantization axes \vec{z}_r and $\vec{z}_{r'}$. (b) f - p transfer integrals. (c) Virtual hopping processes. n (n') and ℓ in the state $f^n p^\ell f^{n'}$ represent the number of f electrons at the Pr site r (r') and that of p electrons at the O1 site.

cal quantization axis \vec{z}_r as this direction, as well as x and y axes as \vec{x}_r and \vec{y}_r depicted in Figs. 1 (a) and (b). The CEF favors $J^z = \pm 4$ configurations for the total angular momentum, which are linearly coupled to $J^z = \pm 1$ and ∓ 2 because of the D_{3d} CEF [18]. This leads to the atomic non-Kramers magnetic ground doublet

$$|\sigma^z\rangle = \alpha|J^z = 4\sigma^z\rangle + \beta\sigma^z|J^z = \sigma^z\rangle - \gamma|J^z = -2\sigma^z\rangle, \quad (1)$$

with small real coefficients β and γ as well as $\alpha = \sqrt{1 - \beta^2 - \gamma^2}$. The pseudospin $\sigma^z = \pm$ represents the direction of the Ising (“in” or “out”) magnetic dipole moment, in contrast to the case of a *nonmagnetic* doublet labeled by the atomic quadrupole moment [19] in materials having other CEF symmetries, $\text{PrFe}_4\text{P}_{12}$ [20], UPt_3 [21], and UPd_2Al_3 [22]. For $\text{Pr}_2\text{Ir}_2\text{O}_7$, the first excited crystal-field level is a singlet located at 168 K and the second is a doublet at 648 K [18]. They are similarly large for $\text{Pr}_2\text{Sn}_2\text{O}_7$ [15]. These energy scales are two orders of magnitude larger than our relevant energy scale $J \sim 1.4$ K. Hence we neglect these CEF excitations.

Now we derive the effective Hamiltonian through the fourth-order strong-coupling perturbation theory. Virtual local f^1 and f^3 states have an energy gain of the Coulomb repulsion U and cost of $2U$, respectively (Fig. 2 (a)), where the LS coupling has been ignored in comparison with U . Creating a virtual p hole decreases the energy by the p electron level Δ compared with the f^1 level. The f - p electron transfer is allowed only within the orbital $l_z = 0$ and ± 1 manifolds, whose amplitudes are given by Slater-Koster parameters $V_{pf\sigma}$ and $V_{pf\pi}$ [23], respectively (Fig. 2 (b)). The local coordinate frames for the nearest-neighbor Pr sites are crucially different; for instance, $\vec{z}_r \cdot \vec{z}_{r'} = -1/3$. The perturbation expansion in $V_{pf\sigma}$ and $V_{pf\pi}$ is then carried out by taking into account the different local coordinate frames and the virtual processes (Fig. 2 (c)). The projection of this superexchange Hamiltonian onto the subspace of doublets (Eq. (1)) leads

to the pseudospin-1/2 Hamiltonian;

$$\begin{aligned} H_{\text{eff}} = J \sum_{\langle r, r' \rangle}^{\text{n.n.}} & [\sigma_r^z \sigma_{r'}^z + 2\delta (\sigma_r^+ \sigma_{r'}^- + \sigma_r^- \sigma_{r'}^+)] \\ & + 2q (e^{i\varphi_{r, r'}} \sigma_r^+ \sigma_{r'}^+ + h.c.), \end{aligned} \quad (2)$$

with $\sigma_r^\pm \equiv (\sigma_r^x \pm i\sigma_r^y)/2$ and $(\sigma_r^x, \sigma_r^y, \sigma_r^z) = \vec{\sigma}_r \cdot (\vec{x}_r, \vec{y}_r, \vec{z}_r)$, where $\vec{\sigma}_r$ represents the Pauli matrix for the pseudospin at the site r . We have adopted the simplest gauge where the phase $\varphi_{r, r'}$ takes 0, $2\pi/3$, $-2\pi/3$ depending on the color of the bond directions shown in Fig. 1 (c), by rotating the x and y axes by $\pi/12$ from those shown in Figs. 1 (a) and (b). This phase can not be fully gauged away, because of the noncollinearity of the $\langle 111 \rangle$ magnetic moments and the three-fold rotational invariance of $(r, \vec{\sigma}_r)$ about the $[111]$ axes. Only σ_r^z contributes to the *magnetic dipole moment* J_r^z , while $\sigma_r^{x,y}$ the *atomic quadrupole moment* $J_r^{x,y}$, as can be shown by direct calculations. For a realistic case $-0.37 \lesssim V_{pf\pi}/V_{pf\sigma} \lesssim -0.02$, the Ising coupling J between the nearest-neighbor pseudospins is found to be positive, i.e., antiferroic. This indicates the “ferromagnetic” coupling between the nearest-neighbor $4f$ magnetic moments because of the tilting of the local z axes, $\vec{z}_r \cdot \vec{z}_{r'} = -1/3$. Then, it can provide a source of the ice-rule formation. The D_{3d} CEF creates two additional quantum-mechanical interactions; the pseudospin-exchange and pseudospin-nonconserving terms. Their coupling constants δ and q are insensitive to $U/V_{pf\sigma}$ and $\Delta/V_{pf\sigma}$ but strongly depends on β and γ . Figure 3 (a) shows δ and q as functions of β for the trigonal CEF with by keeping the ratio $\gamma/\beta = 3$. Henceforth, we adopt rough estimates $U/V_{pf\sigma} = 5$, $\Delta/V_{pf\sigma} = 4$, and $V_{pf\pi}/V_{pf\sigma} = -0.3$ from first-principles calculations (published elsewhere), and $\beta = 7.5\%$ and $\gamma = 3\beta$ from the CEF analysis based on inelastic neutron-scattering experiments [18]. Then, we obtain $\delta \sim 0.51$ and $q \sim 0.89$, indicating the appreciable quantum nature. The two couplings play crucial roles in inducing a cooperative ferroquadrupolar order instead of the classical spin ice [8] or the $U(1)$ spin liquid [24].

A mean-field analysis [5] on Eq. (2) yields two distinct states. (i) Magnetic dipolar states characterized by a nonzero $\langle \sigma_r^z \rangle$ have the lowest energy $-2J$ per tetrahedron at the wavevector $\mathbf{q} = \frac{2\pi}{a}(hhl)$ with a being the side length of the unit cube (Fig. 1 (c)). (ii) A quadrupolar state with a nonzero $\langle \sigma_r^{x,y} \rangle$ has the energy $-2(\delta + 2q)J$ at $\mathbf{q} = 0$ for $\delta, q > 0$. Thus, for $\delta + 2q > 1$ as in our case, the atomic quadrupole moment $\sigma_r^{x,y}$ should form the LRO *without any dipole LRO*. However, we will show below that the ground state is further replaced with a cooperative ferroquadrupolar state because of the quantum interplay between atomic dipoles σ_r^z and quadrupoles $\sigma_r^{x,y}$.

First let us solve Eq. (2) on a single tetrahedron. The similar analysis on a distinct model for $\text{Tb}_2\text{Ti}_2\text{O}_7$ [25] has been employed to discuss the RVB-singlet quantum spin ice [26]. With increasing β and thus γ from

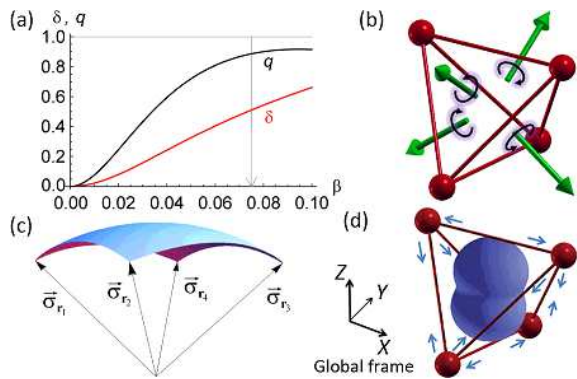


FIG. 3: (Color online) (a) Coupling constants δ and q versus $\beta (= \gamma/3)$. The arrow points to the experimentally estimated value of β [18]. (b) Outward normal vectors (green arrows) of the surfaces of the tetrahedron, used to define the chirality κ_T . (c) Solid angle subtended by four pseudospins $\vec{\sigma}_{r_i}$. (d) Distribution of the tetrahedral magnetic moment \vec{M}_T in the cooperative ferroquadrupolar state ($\langle Q_T^{ZZ} \rangle > 0$). The arrows represent the lattice deformation linearly coupled to Q_T^{ZZ} .

0, three classical levels corresponding to the “2-in, 2-out”, “3-in, 1-out”/“1-in, 3-out” ($\Delta E = 2J$), and “4-in”/“4-out” ($\Delta E = 8J$) configurations are split to three doublets, three triplets, and one singlet. In our case, the ground-state manifold has the E_g symmetry with the double degeneracy $\chi = \pm$ as described as $|\Psi_\chi^s\rangle = \frac{c_2}{\sqrt{6}} \sum_{\tau=\pm} (e^{i\frac{2\pi}{3}\chi} |\tau X\rangle + e^{-i\frac{2\pi}{3}\chi} |\tau Y\rangle + |\tau Z\rangle) + c_4 |4\chi\rangle$ with real coefficients c_2 and c_4 . Here, the orthonormal state $|+4\rangle/|-4\rangle$ represents the “4-in”/“4-out” configuration, while $|\pm X\rangle$, $|\pm Y\rangle$, and $|\pm Z\rangle$ denote the “2-in, 2-out” having the net magnetic dipole moment $\vec{M}_T = M_0 \sum_{\mathbf{r}} \sigma_{\mathbf{r}}^z \hat{z}_{\mathbf{r}}$, pointing to the $\pm X$, $\pm Y$, and $\pm Z$ directions of the global coordinate frame, respectively. We have introduced the moment amplitude $M_0 = gJ\mu_B(4\alpha^2 + \beta^2 - 2\gamma^2) \approx 2.9\mu_B$ with the Landé factor $g_J = 4/5$. The sign $\chi = \pm$ represents the net pseudospin chirality of the tetrahedron, $\kappa_T = \frac{1}{2} \sum_{\mathbf{r}_1, \mathbf{r}_2, \mathbf{r}_3} \vec{\sigma}_{\mathbf{r}_1} \cdot \vec{\sigma}_{\mathbf{r}_2} \times \vec{\sigma}_{\mathbf{r}_3}$, through the relation $\langle \Psi_\chi^s | \kappa_T | \Psi_{\chi'}^s \rangle = \sqrt{3}c_2^2 \chi \delta_{\chi, \chi'}$. Here, the summation over the sites $\mathbf{r}_1, \mathbf{r}_2, \mathbf{r}_3$ on the tetrahedron T is taken so as they appear counterclockwise about the outward normal to the plane spanned by the three sites (Fig. 3 (b)). This κ_T gives the solid angle subtended by the four pseudospins (Fig. 3 (c)). Note that the “2-in, 2-out” singlet state with the A_{1g} symmetry [26], $\sum_{\tau=\pm} (|\tau X\rangle + |\tau Y\rangle + |\tau Z\rangle)/\sqrt{6}$, is located at a high energy $\Delta E \sim 7J$. The triply degenerate first excited states consist of only “3-in, 1-out” and “1-in, 3-out”, and are located at $\Delta E \sim J$. In fact, any eigenstate of the single-tetrahedron Hamiltonian is described by either “3-in, 1-out” and “1-in, 3-out” configurations or “2-in, 2-out” and “4-in”/“4-out” configurations. Therefore, quantum effects of creating “3-in, 1-out” and “1-in, 3-out” configurations from the “2-in, 2-out” can not be taken into

account in the single-tetrahedron analysis.

To overcome this drawback, we numerically solve the model for the 16-site ($N = 16$) cubic cluster with the periodic boundary condition (Fig. 1 (c)). It is found that the ground states have a six-fold degeneracy labeled by the inversion (I) even(+)/odd(-) and the wavevector $\mathbf{k}_X = (\frac{2\pi}{a}, 0, 0)$, $\mathbf{k}_Y = (0, \frac{2\pi}{a}, 0)$, or $\mathbf{k}_Z = (0, 0, \frac{2\pi}{a})$ with the energy $\sim -8.825J$ per tetrahedron. The states associated with \mathbf{k}_i have a cooperative quadrupole moment defined on each tetrahedron, $\langle Q_T^{ii} \rangle = 0.0387M_0^2$, where $Q_T^{ij} = 3M_T^i M_T^j - \vec{M}_T^2 \delta_{ij}$ with $i, j = X, Y, Z$. Namely, the net magnetic moment \vec{M}_T in each tetrahedron T points, for instance, to the $\pm Z$ directions with a higher probability than to the $\pm X$ and $\pm Y$ (Fig. 3 (d)). Such ferroquadrupole order spontaneously breaking the three-fold rotational invariance about the $[111]$ axes can occur in the thermodynamic limit. This ferroquadrupole moment Q_T^{ii} linearly couples to a lattice vibration: the four ferromagnetic bonds and the two antiferromagnetic bonds should be shortened and expanded, respectively, leading to a crystal symmetry lowering from cubic to tetragonal accompanied by a compression in the direction of the ferroquadrupole moment (Fig. 3 (d)). This state shows both axial alignments of magnetic dipoles and a broken translational symmetry, and can then be classified into a magnetic analog of a smectic (or crystalline) phase of liquid crystals [17]. Such magnetic quadrupole correlations in $\text{Pr}_2\text{TM}_2\text{O}_7$ could be probed by NMR experiments.

Next, we calculate the magnetic dipole correlation, $S(\mathbf{q}) = \frac{M_0^2}{N} \sum_{\mathbf{r}, \mathbf{r}'} (\delta_{ij} - \frac{q_i q_j}{|\mathbf{q}|^2}) z_{\mathbf{r}}^i z_{\mathbf{r}'}^j \langle \sigma_{\mathbf{r}}^z \sigma_{\mathbf{r}'}^z \rangle_{\text{ave}} e^{i\mathbf{q} \cdot (\mathbf{r} - \mathbf{r}')}$, averaged over the six-fold degenerate ground states. This quantity is relevant to the neutron-scattering intensity integrated over the low-energy region below the crystal-field excitations from the atomic ground doublet Eq. (1). Note that neutron spins do not couple to $\sigma_{\mathbf{r}}^\pm$ which represents the atomic quadrupole. Figure 4 (a) shows the profile of $S(\mathbf{q})$ for $\mathbf{q} = \frac{2\pi}{a}(hhl)$. It exhibits intense peaks at (001) and (003), weaker peaks at $(\frac{3}{4}\frac{3}{4}0)$, and the minimum at (000), as in the dipolar spin ice [8], though the peaks are broadened by the quantum fluctuations in this ferroquadrupolar state. Besides, the nonzero q term in the Hamiltonian partially violates the ice rule and eliminates the pinch-point singularity [27, 28] observed at (111) and (002) in the spin ice [29], which should be examined by large system-size calculations. Note that our magnetic profile reproduces powder neutron-scattering results on $\text{Pr}_2\text{Sn}_2\text{O}_7$ [15] that reveal the enhanced low-energy short-ranged intensity at $q \sim \frac{2\pi}{a} \sim 0.5 \text{ \AA}^{-1}$ with a shoulder at $q \sim \frac{6\pi}{a}$ (Fig. 4(b)). This experiment also shows a saturation of the quasielastic peak width $\sim 0.1 \text{ meV} \sim J$ at 0.2 K [15]. Such large spin relaxation rate can be attributed to the appreciable quantum nature; large δ and q in Eq. (2). These agreements support our scenario of the quantum melting of a spin ice.

Now we concentrate on the ground states having the

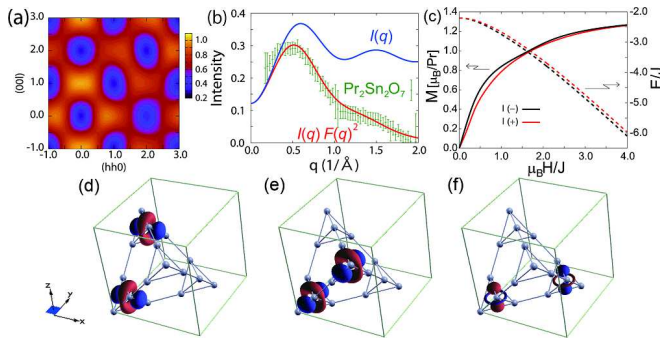


FIG. 4: (Color) (a) $S(\mathbf{q})/M_0^2$ constructed from the local, nearest-neighbor, and second-neighbor correlations. (b) The theoretical curve (red) $I(q)F(q)^2$ with the form factor $F(q)$ and the experimental data (green) of the powder neutron-scattering intensity on $\text{Pr}_2\text{Sn}_2\text{O}_7$ at 1.4 K [15]. $I(q)$ (blue curve) is the angle average of $S(\mathbf{q})/M_0^2$. (c) The magnetizations (left) and energies (right) per site for the I -odd(-) ground state and the I -even(+) state under the magnetic field $\vec{H} \parallel \langle 111 \rangle$. (d-f) Quadrupole correlations $\langle Q_T^{ii} Q_{T'}^{jj} \rangle$ between the tetrahedrons T and T' displaced by $\mathbf{r} = \mathbf{r}_X$ (d), \mathbf{r}_Y (e), and \mathbf{r}_Z (f) in the cooperative ferroquadrupolar state with the wavevector \mathbf{k}_Z and $\langle Q_T^{ZZ} \rangle \neq 0$. The matrix $\langle Q_T^{ii} Q_{T'}^{jj} \rangle$ in i, j has been diagonalized to yield two orthogonal forms of quadrupoles, $\mathcal{Q}_{r\mu} = \sum_i \lambda_{r\mu}^i Q_T^{ii}$ ($\mu=1,2$). The shape of \mathcal{Q}_{r1} showing the dominant correlation amplitude is shown. Red/blue regions represent positive/negative values of \mathcal{Q}_{r1} .

quadrupole moment $\langle Q_T^{ZZ} \rangle > 0$ and the associated wavevector \mathbf{k}_Z . The magnetic susceptibility is finite in the ferroquadrupolar state, as seen from the slope of the magnetization curve along the $\langle 111 \rangle$ direction in Fig. 4 (c). This indicates a negative T_{CW} as found in $\text{Pr}_2\text{Zr}_2\text{O}_7$ [12] and $\text{Pr}_2\text{Ir}_2\text{O}_7$ [14], and the absence of an internal magnetic field as in $\text{Pr}_2\text{Ir}_2\text{O}_7$ [16]. The magnetic field lifts the degeneracy due to the I symmetry. The ground-state (I -odd) magnetization shows a small step or dip around $\mu_B H/J \sim 1.5$, in comparison with that of the I -even excited state. This indicates that the structure develops upon cooling. These agree with the experimental observation on $\text{Pr}_2\text{Ir}_2\text{O}_7$; $M \sim 0.8\mu_B$ at the metamagnetic transition $\mu_B H_c/J \sim 1.3$ with $J \sim 1.4$ K [14].

Finally we spatially resolve the multipolar correlations within the cubic unit cell. Figures 4 (d), (e), and (f) represent quadrupole correlations $\langle Q_T^{ii} Q_{T'}^{jj} \rangle$ between the tetrahedrons T and T' displaced by $\mathbf{r}_X = (0, \frac{a}{2}, \frac{a}{2})$, $\mathbf{r}_Y = (\frac{a}{2}, 0, \frac{a}{2})$, and $\mathbf{r}_Z = (\frac{a}{2}, \frac{a}{2}, 0)$, respectively. There exist dominant ferroquadrupolar correlations shown in Figs. 4 (d) and (e), both of which favor ferroquadrupole moments along the Z direction. They prevail over subdominant antiferroquadrupole correlations shown in Fig. 4 (f), and are responsible for the ferroquadrupole order $\langle Q_T^{ZZ} \rangle \neq 0$. On the other hand, the chirality correlation $\langle \kappa_T \kappa_{T'} \rangle$ is weakly ferrochiral between the tetrahedrons shown in Figs. 4 (d) and (e), while it is strongly antiferrochiral between those shown in Fig. 4 (f). This

points to a geometrical frustration suppressing the chirality LRO in each fcc sublattice of the diamond lattice formed by the tetrahedrons. Further studies are required for examining a possibility of a chiral spin liquid [3]. The broken time-reversal symmetry without magnetic dipole LRO, reported in $\text{Pr}_2\text{Ir}_2\text{O}_7$ [14], might be detected even in insulating magnets such as $\text{Pr}_2\text{Zr}_2\text{O}_7$ and $\text{Pr}_2\text{Sn}_2\text{O}_7$ through magneto-optical Kerr-effect measurements.

The proposed scenario of the quantum melting of the spin ice explains magnetic properties observed in $\text{Pr}_2\text{TM}_2\text{O}_7$. Effects of coupling of localized f -electrons to conduction electrons on the transport properties are left for a future study. The orbital motion of conduction electrons can flip the pseudospin-1/2. This could be an origin of the resistivity minimum observed in $\text{Pr}_2\text{Ir}_2\text{O}_7$ [13].

The authors thank S. Nakatsuji, Y. Machida, Y. B. Kim, K. Matsuhira, and D. MacLaughlin for discussions. The work was supported by Grants-in-Aid for Scientific Research under No. 19052006, 20029006, and 20046016 from the MEXT of Japan and 21740275 from the JSPS.

-
- [1] P. W. Anderson, Phys. Rev. **102**, 1008 (1956).
 - [2] P. W. Anderson, Mater. Res. Bull. **8**, 153 (1973).
 - [3] X. G. Wen *et al.*, Phys. Rev. B **39**, 11413 (1989).
 - [4] P. A. Lee, Science **321**, 1306 (2009).
 - [5] J. N. Reimers *et al.*, Phys. Rev. B **43**, 865 (1991).
 - [6] M. J. Harris *et al.*, Phys. Rev. Lett. **79**, 2554 (1997).
 - [7] A. P. Ramirez *et al.*, Nature (London) **399**, 333 (1999).
 - [8] S. T. Bramwell and M. J. P. Gingras, Science **294**, 1495 (2001).
 - [9] C. Castelnovo *et al.*, Phys. Rev. Lett. **104**, 107201 (2010).
 - [10] J. Rossat-Mignod, in *Proceedings of the Nato Advanced Study Institute on Systematics and the Properties of the Lanthanides*, Chap. 7, ed. S. P. Sinha (Reidel, Dordrecht, 1983).
 - [11] K. Matsuhira *et al.*, J. Phys. Soc. Jpn. **71**, 1576 (2002).
 - [12] K. Matsuhira *et al.*, J. Phys.: Conf. Series **145**, 012031 (2009).
 - [13] S. Nakatsuji *et al.*, Phys. Rev. Lett. **96**, 087204 (2006).
 - [14] Y. Machida *et al.*, Nature (London) **463**, 210 (2010).
 - [15] H. D. Zhou *et al.*, Phys. Rev. Lett. **101**, 227204 (2008).
 - [16] D. E. MacLaughlin *et al.*, Physica B **404**, 667 (2009).
 - [17] P. G. de Gennes and J. Prost, *The Physics of Liquid Crystals*, 2nd ed. (Clarendon, Oxford, 1993).
 - [18] Y. Machida, Ph. D thesis, Kyoto University (2006).
 - [19] D. L. Cox, Phys. Rev. Lett. **59**, 1240 (1987).
 - [20] Y. Aoki *et al.*, Phys. Rev. B **65**, 064446 (2002).
 - [21] R. Joynt and L. Taillefer, Rev. Mod. Phys. **74**, 235 (2002).
 - [22] A. Grael *et al.*, Phys. Rev. B **46**, (1992) 5818.
 - [23] R. R. Sharma, Phys. Rev. B **19**, 2813 (1979).
 - [24] M. Hermele *et al.*, Phys. Rev. B **69**, 064404 (2004).
 - [25] J. S. Gardner *et al.*, Phys. Rev. Lett. **82**, 1012 (1999).
 - [26] H. R. Molavian *et al.*, Phys. Rev. Lett. **98**, 157204 (2007).
 - [27] S. V. Isakov *et al.*, Phys. Rev. Lett. **93**, 167204 (2004).
 - [28] C. L. Henley, Phys. Rev. B **71**, 014424 (2005).
 - [29] D. J. P. Morris *et al.*, Science **326**, 411 (2009); T. Fennell *et al.*, Science **326**, 415 (2009).